

Cluster scaling relations from cosmological hydrodynamic simulations in dark energy dominated universe

N. Aghanim¹, A. C. da Silva^{1,2}, and N. J. Nunes³

¹ IAS, CNRS & Université Paris Sud, Bâtiment 121, 91405 Orsay, France
e-mail: nabila.aghanim@ias.u-psud.fr

² Centro de Astrofísica, Universidade do Porto, Rua das Estrelas, 4150-762 Porto, Portugal
e-mail: asilva@astro.up.pt

³ Department of Applied Mathematics and Theoretical Physics, Wilberforce Road, Cambridge, CB3 0WA, UK
e-mail: nunes@damtp.cam.ac.uk

ABSTRACT

Context. Clusters are potentially powerful tools for cosmology provided their observed properties such as the Sunyaev-Zel'dovich (SZ) or X-ray signals can be translated into physical quantities like mass and temperature. Scaling relations are the appropriate mean to perform this translation. It is therefore, important to understand their evolution and their modifications with respect to the physics and to the underlying cosmology.

Aims. In this spirit, we investigate the effect of dark energy on the X-ray and SZ scaling relations. The study is based on the first hydro-simulations of cluster formation for different models of dark energy. We present results for four dark energy models which differ from each other by their equations of state parameter, w . Namely, we use a cosmological constant model $w = -1$ (as a reference), a perfect fluid with constant equation of state parameter $w = -0.8$ and one with $w = -1.2$ and a scalar field model (or quintessence) with varying w .

Methods. We generate N -body/hydrodynamic simulations that include radiative cooling with the public version of the Hydra code, modified to consider an arbitrary dark energy component. We produce cluster catalogues for the four models and derive the associated X-ray and SZ scaling relations.

Results. We find that dark energy has little effect on scaling laws making it safe to use the Λ CDM scalings for conversion of observed quantities into temperature and masses.

Key words. cosmology, galaxies: clusters, methods: numerical

1. Introduction

In order to explain the current acceleration of the universe (Riess et al. 1998; Perlmutter et al. 1999) in the context of the theory of General Relativity, it is general procedure to introduce a new form of gravitational component with negative pressure – dark energy. Various candidates such as a cosmological constant or a quintessence field have been proposed. These models are characterised by their equation of state parameter and constrained by either using the observation of background quantities or the growth of cosmic structures. An alternative way to explain the acceleration of the universe is to allow for modifications of gravity. Many classes of models exist, for instance, a light scalar field coupled to matter leads to models of extended quintessence and more generally to scalar-tensor type theories. Further possibilities were studied in the context of braneworld models. Testing the Poisson equation on large scales may be a way to distinguish between all these alternative scenarios.

Regardless of its nature, dark energy as a dominant component, plays a role in structure formation and thus modifies the number of formed structures. The evolution of linear perturbations in the presence of a scalar field like quintessence and the effects on the abundance of collapsed structures and its dependence with redshift were widely

explored and suggested as a tool to constrain the nature of dark energy and its evolution, e.g. (Haiman et al. 2001; Weller et al. 2001; Weinberg & Kamionkowski 2003; Battye & Weller 2003; Wang et al. 2004; Mohr 2004). The properties of collapsed halos (density contrast and virial radius) depend strongly on the shape of the potential, the initial conditions, the time evolution of the dark energy equation of state and on its ability to collapse at the structure scale, e.g. (Nunes & Mota 2006). One can additionally investigate the effects of dark energy on the growth rate of structure and consequently study how dark energy affects the abundance of collapsed halos in dark energy models, e.g. (Nunes et al. 2006; Manera & Mota 2006).

Cluster number counts can potentially discriminate between dark energy models, in particular, the evolution of their equation of state. However, a large number of clusters with known redshifts from SZ, X-ray or optical surveys are needed, e.g. (Bartelmann et al. 2005). Future Sunyaev-Zel'dovich (SZ) as well as X-rays observations will provide us with high quality data making galaxy clusters an efficient and powerful cosmological tool. Cluster physics, however, is complex. The presence of substructures, the possible contamination by radio and IR sources, the still imperfect knowledge of the relation between the halo mass and the clusters observed properties induce degeneracies between cluster physics and cosmological models. Scaling relations are key quantities in observational cosmology as they re-

late the observables in X-rays and SZ to the cluster properties, namely, masses and temperatures. The latter are then used in cluster number counts to constrain the cosmological models.

Due to their importance in translating observations to physical quantities, but most of all in probing the cluster formation, scaling relations have raised considerable attention. Simple models of formation of virialised systems such as clusters predict that they exhibit self-similar behaviours (Kaiser 1986), see also (Ascasibar et al. 2006). In the self-similar model, gravitational infall drives shock heating of the intra-cluster medium (ICM) and establishes the gas properties such that they scale with the halo mass giving rise to the scaling relations. However, it is now clear that additional physics is required to provide a more complete picture of the cluster formation and evolution, and to explain the deviations between observations and the predictions based on self-similar scaling as shown mostly by X-ray observations (Edge & Stewart 1991; Allen & Fabian 1998; Markevitch 1998; Nevalainen et al. 2000; Finoguenov et al. 2001; Ettori et al. 2004; Henry 2004; Arnaud et al. 2005; Rasia et al. 2005; Balogh et al. 2006; Maughan et al. 2006; Morandi et al. 2007). As the complexity of the physical description increases due to the additional gas physics (galactic winds and/or quasar outflows, radiative cooling, preheating) the use of numerical simulations appears the best option to compare predictions and observations and examine the role of those new ingredients in explaining the departures from self-similarity (e.g. (Evvard et al. 1996; Bryan & Norman 1998; Bialek et al. 2001; Thomas et al. 2001; Babul et al. 2002; Voit et al. 2002; Borgani et al. 2004; Rowley et al. 2004; Muanwong et al. 2006; Kay et al. 2007)). The ICM can additionally be probed by the Sunyaev-Zel'dovich (SZ) effect, inverse Compton scattering of cosmic microwave background (CMB) photons off high energy electrons. The magnitude of the SZ effect is determined by the integrated gas pressure along the line-of-sight, called the Compton parameter, y . Unlike the X-ray surface brightness, the SZ effect is not subject to cosmological dimming and can be used out to high redshift which makes SZ scaling relations particularly interesting and attractive tests. Nevertheless, SZ measurements, although gaining in quality and quantity, are at the moment still not sufficient to be fully used and this explains why investigations of SZ scaling relations are still limited from the observational point of view (Cooray 1999; Benson et al. 2004; McCarthy et al. 2003; Morandi et al. 2007) as well as from the numerical point of view (da Silva et al. 2004; Molt et al. 2005; Bonaldi et al. 2007).

Scaling laws relate the observed properties in X-rays and SZ to the cluster properties, namely, masses and temperatures which are then used to construct mass functions and number counts utilised to constrain the cosmological models. Understanding the possible biases in the scaling relations is thus essential for the use of clusters as cosmological probes. Previous studies, based on numerical simulations, have focused on the effects of additional gas physics in the scaling laws. In the present study, we explore the effects of the cosmological model on the scaling properties of galaxy clusters and their evolutions. We perform hydrodynamic numerical simulation of cluster formation and evolution assuming a simple radiative cooling model, rather than a more complete gas model, which allow us to single out

only dark energy properties. We then investigate whether the X-ray and SZ scaling laws derived for different dark energy models depart from those obtained in the standard cosmological constant model (the Λ CDM model) taken as our reference. In the next section we briefly present the dark energy models used for the first numerical simulation of cluster formation with hydrodynamics in dark energy dominated universes. We describe the simulation code and the procedure used to construct the X-ray and SZ cluster catalogues. In Sect. 3, we present the X-ray and SZ scaling laws studied in the article together with the fitting procedure. Our results and conclusions are summarised in Sect. 4 and 5 respectively.

2. Dark-energy simulations

2.1. Simulation models

Numerical N-body simulations including a dark energy component were performed by several groups to complement the analytical computations of structure formation in presence of dark energy, and to the study the effects of dark energy at the structure level. All studies on galaxy clusters, were essentially dedicated to study dark matter halo shapes and mass functions in different models of dark energy (Linder & Jenkins 2003; Lokas et al. 2003; Klypin et al. 2003; Dolag et al. 2004; Kuhlen et al. 2004). The overall picture that has emerged from these studies is that halo mass functions are well approximated by the Jenkins mass function (Jenkins et al. 2001) and halo core densities, or concentrations, are sensitive to the mean cosmological density at halo formation and therefore depend on the underlying dark-energy model. These findings have led to investigations of the effect of dark energy on the lensing properties of simulated cluster sized halos and their possible use to constrain dark energy, see e.g. (Meneghetti et al. 2005b; Meneghetti et al. 2005a). In the present study we perform the first hydrodynamics simulation of cluster formation in dark energy dominated universe and we focus, for the first time, on the baryonic component of clusters and investigate the possible effects of dark energy on their gas properties. In an earlier study, (Maio et al. 2006) produced numerical simulations of dark energy with baryonic gas to study the implications on cosmic reionisation from first stars.

In all the aforementioned studies, the scalar field associated with dark energy is assumed not to have density fluctuations on scales of galaxy clusters or below. If dark energy influences the perturbations on small scales as proposed for example by (Arbey et al. 2001), (Bean & Magueijo 2002), (Padmanabhan & Choudhury 2002) or (Bagla et al. 2003), the collapse of structures itself will be affected. In our simulations, we will also ignore any possibility for dark energy to cluster and influence the cluster formation.

In addition to the cosmological constant model with a constant equation of state parameter $w = \rho_{\text{de}}/P_{\text{de}} = -1$, we simulate four other models previously studied in (Nunes et al. 2006). These phenomenological models span the range of values that the equation of state parameter can take for typical quintessence models and are compatible with current observational constraints. We take two models for which the dark energy is given by a perfect fluid with constant equation of state parameter: $w = -0.8$ and $w = -1.2$ (phantom dark energy), and

one model where dark energy results from a slowly evolving scalar field in a potential with two exponential terms (2EXP1) (Barreiro et al. 2000)

$$V(\phi) = V_0 (e^{\alpha\kappa\phi} + e^{\beta\kappa\phi}), \quad (1)$$

where $\alpha = 6.2$ and $\beta = 0.1$ which has equation of state parameter today $w_0 = -0.95$. One other model (2EXP2) with varying equation of state was studied in (Nunes et al. 2006). However, because its energy contribution to the total energy of the universe quickly decays with redshift it has no significant departures from the Lambda model in the redshift range of cluster formation (e.g. $z < 5$). We thus choose, from this point onwards, not to consider this model in this work. We further assume for all models that energy density of dark energy, dark matter and baryons today are respectively $\Omega_{\text{de}} = 0.7$, $\Omega_{\text{m}} = 0.3$, $\Omega_{\text{B}} = 0.0486$ and the Hubble parameter $h = H_0/100 \text{ km s}^{-1} \text{ Mpc}^{-1} = 0.7$. $\sigma_8 = 0.9$.

2.2. The simulation code

For each of the cosmological models considered, we performed N -body/hydrodynamic simulations of structure formation using a modified version of the public **Hydra** code (Couchman et al. 1995; Pearce & Couchman 1997), which implements an adaptive particle-particle/particle-mesh (AP³M) algorithm to calculate gravitational forces (Couchman 1991) and smoothed particle hydrodynamics (SPH) (Monaghan 1992) to estimate hydrodynamic quantities. The SPH implementation follows that used by (Thacker & Couchman 2000) and conserves both energy and entropy. All simulations included a model for radiative cooling using the method described in (Thomas & Couchman 1992) and based on the cooling tables of (Sutherland & Dopita 1993). The metallicity was assumed to be a global time varying quantity, $Z = 0.3(t/t_0)Z_{\odot}$, where t/t_0 is the age of the universe in units of the current time and Z_{\odot} is the solar metallicity. At a given time step, gas particles with temperatures below $1.2 \times 10^4 \text{ K}$ and overdensities (relative to the critical) larger than 10^4 , are converted into collisionless material and no longer participate in the gas dynamical processes.

We modified the computation of the physical time, t , and scale factor, a , in **Hydra** to account for the effect of time-variable equations of state of dark energy,

$$t = \int_0^a \frac{da'}{a' H(a')} = H_0^{-1} \int_0^a \frac{d \ln a'}{E(a')}, \quad (2)$$

where $E(a) \equiv H(a)/H_0$, or

$$E(a)^2 = \frac{\Omega_{\text{m}}}{a^3} + \Omega_{\text{de}} e^{-3 \int_a^1 (1+w(a')) \frac{da'}{a'}} + \frac{1 - \Omega_{\text{m}} - \Omega_{\text{de}}}{a^2}, \quad (3)$$

for flat cosmologies. To speed up computations, this quantity is pre-tabulated for each of the dark energy models and read once at the beginning of the simulation run. $E(a)$ is then interpolated and used in Eq. (2). With these modifications our version of the **Hydra** code can thus be used to simulate generic models of homogeneous dark energy.

The initial density field of simulations was constructed, at redshift $z = 49$, using $N = 4,096,000$ particles of baryonic and dark matter, perturbed from a regular grid of fixed

comoving size $L = 100 h^{-1} \text{ Mpc}$. We use the Zel'dovich approximation and the same set of random numbers to generate the initial displacements. The amplitude of the matter power spectrum was calculated assuming $\sigma_8 = 0.9$ in all models and the linear growth factor computed for each model, as presented in (Nunes & Mota 2006). We refer the reader to this article for a discussion on the normalisation. We also assume that the matter power spectrum transfer function is the same for all models and equals that of the cosmological constant model, which is computed using the BBKS formula (Bardeen et al. 1986) and the shape parameter Γ given by the formula in (Sugiyama 1995). With this choice of parameters, the dark matter and baryon particle masses are $2.1 \times 10^{10} h^{-1} \text{ M}_{\odot}$ and $2.6 \times 10^9 h^{-1} \text{ M}_{\odot}$ respectively. In physical units the gravitational softening was set fixed to $25 h^{-1} \text{ kpc}$ below $z = 1$ and above this redshift scaled as $50(1+z)^{-1} h^{-1} \text{ kpc}$.

Individual simulation runs took between 2592 to 2812 time steps to evolve to $z = 0$. For each run we stored a total of 50 simulation snapshots (box outputs) at a list of selected redshifts (the same to all runs) ranging from $z = 20$ to $z = 0$. Thirty of these outputs are inside the interval $0 < z < 3$, which is typically the range where galaxy clusters form.

2.3. Catalogue construction

From simulations, we constructed cluster catalogues using a modified version of the cluster extraction software developed at Sussex by Thomas and collaborators (Thomas et al. 1998; Pearce et al. 2000; Muanwong et al. 2001). To summarize, the cluster identification process starts with the construction of a minimal-spanning tree of dark matter particles whose density exceeds the mean density of the box by $\Delta_{\text{b}} = 178 \times \Omega_{\text{m}}^{-0.55}(z)$ (i.e., the density contrast predicted by the spherical collapse model of a virialised sphere relative to the mean background density in the Lambda cosmology (Eke Navarro & Frenk 1998)). Although Δ_{b} may differ for different dark-energy models, this is not important at this step because cluster properties are computed at fixed overdensities as described below. The minimal-spanning tree is then split into clumps of particles using a maximum linking length equal to $0.5 \Delta_{\text{b}}^{-1/3}$ times the mean inter-particle separation. Finally we grow a sphere around the densest dark matter particle in each clump until the enclosed mass verifies

$$M_{\Delta}(< R_{\Delta}) = \frac{4\pi}{3} R_{\Delta}^3 \Delta \rho_{\text{crit}}(z), \quad (4)$$

where Δ is a fixed overdensity contrast, $\rho_{\text{crit}}(z) = (3H_0^2/8\pi G)E^2(z)$ is the critical density and $E(z)$ is given by Eq. (3). We have constructed master catalogues for all dark-energy simulation containing at least 500 particles of gas and dark matter, i.e. with an equivalent minimum mass of $M_{\text{lim}} \approx 1.18 \times 10^{13} h^{-1} \text{ M}_{\odot}$, at four fixed overdensities, $\Delta = 200, 500, 1000, 2500$. Here we will report our findings for cluster scaling relations only at $\Delta = 200$, the largest cluster overdensity radius usually considered in the literature. For this catalogue we find 377, 393, 396, 374 clusters at $z = 0$ in the cosmological constant, $w = -0.8$, 2EXP1 and $w = -1.2$ simulation runs respectively. Although our choice of Δ_{b} may limit exact comparison of numbers, these abundances reproduce the behaviour predicted in

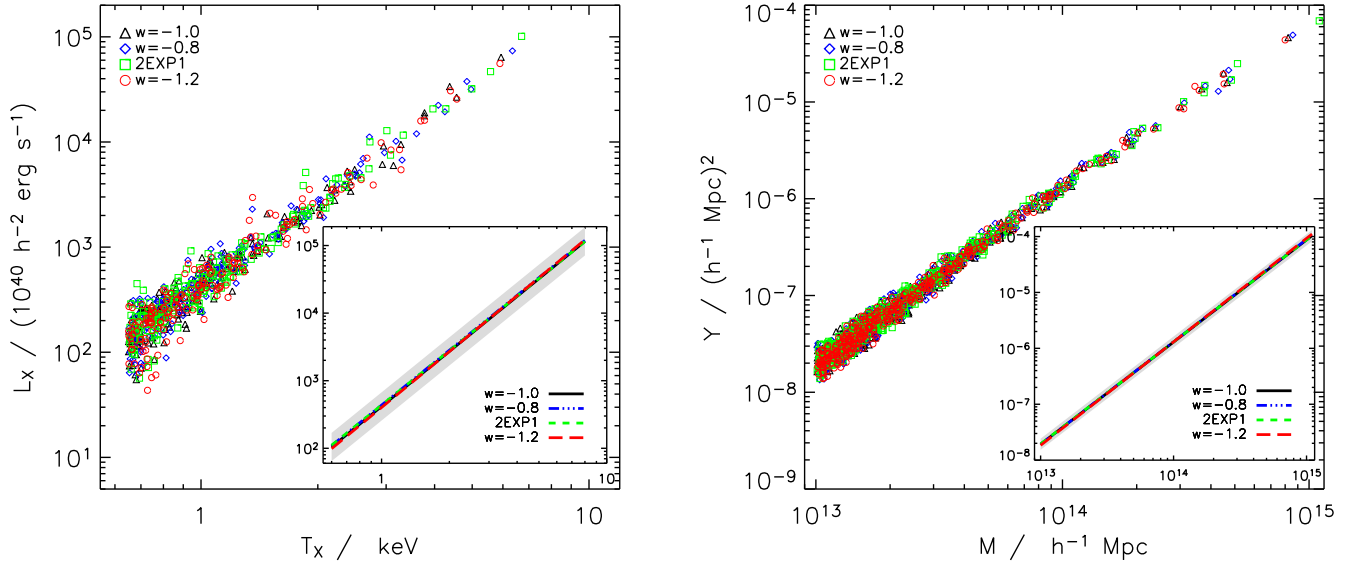


Fig. 1. Cluster scaling relations $L_{X,200} - T_{X,200}$ (left panel) and $Y_{200} - M_{200}$ (right panel) at redshift zero. Displayed quantities are computed within R_{200} , the radius where the mean cluster density is 200 times larger than the critical density. The embedded plots show the best fits with a power law to clusters represented in the main plots for the $w = -1$ (triangles), $w = -0.8$ (diamonds), 2EXP1 (squares) and $w = -1.2$ (circles) models. The shaded regions in the embedded plots give the typical scatter of the fits, i.e. the r.m.s dispersion around the best fit lines.

(Nunes et al. 2006) in their analytical study. We note that the cluster definition used in this paper is different from that used in (da Silva et al. 2004; Muanwong et al. 2006). Despite the similar simulation parameters, direct comparison with their findings is only possible for the Lambda model at redshift zero, where cluster definitions are identical.

For each model, the cluster catalogue provides us with estimated structural and observable quantities. More specifically for this study we compute: masses; intrinsic SZ luminosity, $Y = Y_{\text{SZ}} \times D_A^2$ where Y_{SZ} is the integrated SZ signal and D_A is the angular diameter distance; mass-weighted gas temperature T_{mw} ; and bolometric X-ray temperature, T_X , and luminosity, L_X , excluding a cooling radius of about $50 h^{-1} \text{kpc}$ around the cluster centre. We refer the reader to (da Silva et al. 2004) for the definitions of the these quantities.

3. Analysis of the scaling relations

In this paper we investigate the following scaling relations between cluster properties: $T_X - M$, $Y - M$, $Y - T_{\text{mw}}$, $L_X - T_X$, and $Y - L_X$. These can be expressed as:

$$T_X = A_{\text{TM}} (M/M_0)^{\alpha_{\text{TM}}} (1+z)^{\beta_{\text{TM}}} E(z)^{2/3}, \quad (5)$$

$$Y = A_{\text{YM}} (M/M_0)^{\alpha_{\text{YM}}} (1+z)^{\beta_{\text{YM}}} E(z)^{2/3}, \quad (6)$$

$$Y = A_{\text{YT}} (T_{\text{mw}}/T_{\text{mw},0})^{\alpha_{\text{YT}}} (1+z)^{\beta_{\text{YT}}} E(z)^{-1}, \quad (7)$$

$$L_X = A_{\text{LT}} (T_X/T_{X,0})^{\alpha_{\text{LT}}} (1+z)^{\beta_{\text{LT}}} E(z), \quad (8)$$

$$Y = A_{\text{YL}} (L_X/L_{X,0})^{\alpha_{\text{YL}}} (1+z)^{\beta_{\text{YL}}} E(z)^{-9/4}, \quad (9)$$

where we have chosen the normalisation scales $M_0 = 10^{14} h^{-1} M_\odot$, $T_{X,0} = T_{\text{mw},0} = 1 \text{ keV}$, $L_{X,0} = 10^{43}$

erg/s/h^2 . The powers of the $E(z)$ function give the predicted evolution, extrapolated from the self-similar model, (Kaiser 1986), of the scalings in each case. The quantities, A , α , and β , give: the scalings normalisation at $z = 0$; the power on the independent variable; and the departures from the expected redshift evolution.

To investigate these cluster scaling relations in our simulations we use the method described in (da Silva et al. 2004). According to Eqs. (5-9), the general form of how a given cluster property y relates to a property x can be written as,

$$y f(z) = y_0(z) (x/x_0)^\alpha, \quad (10)$$

where

$$y_0(z) = A (1+z)^\beta, \quad (11)$$

and $f(z)$ is some fixed power of the cosmological factor $E(z)$. This is a power-law function whose parameters A , α and β can be obtained by fitting our cluster catalogue distributions at each redshift with a straight line in the $(\log(y f(z)), \log x)$ plane. To be more specific, the fitting procedure is carried out in three steps. Firstly, we fit the cluster distributions with a straight-line in logarithmic scale at all redshifts. If the logarithmic slope α remains approximately constant (i.e. shows no systematic variations) within the redshift range of interest, we then take α at $z = 0$ as the best fit value. In the second step, we repeat the fit using this value of α to determine the scaling normalisation factors $y_0(z)$. This avoids unwanted correlations between α and $y_0(z)$. Finally, in the last step we use Eq. (11) to obtain the parameters A and β .

In the fitting process we consider only clusters with $M_{\text{lim}} > 5 \times 10^{13} h^{-1} M_\odot$ for scalings with mass, $L_{\text{lim}} > 6.6 \times 10^{42} h^{-2} \text{ erg s}^{-1}$ for scalings with luminosity, and $T_{\text{mw,lim}} > 1 \text{ keV}$, $T_{X,\text{lim}} > 1.1 \text{ keV}$ for scalings with mass-weighted and emission-weighted temperatures, respectively.

This ensures that our cluster samples are complete at all redshifts and that, for each model, equal number of clusters are used for all scalings at redshift zero. With these selection criteria our cluster samples contain 60 clusters for the cosmological constant model, and a similar number of clusters for the other models, at $z=0$. We note that above $z = 1.5$ the number of clusters with $M_{\text{lim}} > 5 \times 10^{13} h^{-1} M_{\odot}$ in our sample decreases typically below 10, hence, we do not fit the scaling relations above this redshift value. As we will discuss in the next section, all the scaling relations explored in the present study, are well fitted by power-laws of the form Eq. (10), in the redshift range $0 < z < 1.5$, except for the $L_X - T_X$ and $Y - L_X$ whose normalization dependences with redshift, $\log(y_0(z))$, are well approximated by a straight line only in a narrower redshift range.

4. Results

4.1. Scaling relations at $z = 0$

We start by discussing the cluster scaling laws at redshift zero. These were determined, for all scalings and models under investigation in this work, at an overdensity radius R_{200} . In Table 1 we present the power law best fit for the logarithmic slopes α obtained for each of the cases. As can be inferred from the table, all models provide very similar results for each scaling, with differences between models being comparable or in most cases within the statistical errors of the fit. This indicates that the local cluster scaling relations are quite insensitive to the underlying dark energy model driving the present-day evolution of the universe. As stated in Sec. 2.3, our cluster definition is the same as in (da Silva et al. 2004; Muanwong et al. 2006) (only) at redshift zero, for the Lambda model. We verified that indeed theirs and our results are in excellent agreement at this redshift.

To illustrate the robustness of the scalings with respect to the dark energy models investigated in this paper, we present in Figure 1 two characteristic X-ray and SZ galaxy cluster scaling relations: the $L_X - T_X$ (left panel) and the $Y - M$ (right panel) scalings. In each case, the main plot shows the cluster distributions for all models whereas the embedded panels show the power law best fits obtained. For both scaling relations, the cluster distributions and best fit lines clearly overlap. Also represented by a shaded area in the embedded panels is the r.m.s. dispersion of the fit for Lambda model:

$$\sigma_{\log y'} = \sqrt{\frac{1}{N} \sum_i (\log(y'_i/y'))^2}, \quad (12)$$

where $y' = yf$ (see Eq. (10)) and y'_i are individual data points. This dispersion is of the same size of the fit dispersions obtained in the other models and it is clearly wider than the best fit line separations of the various dark energy models. As expected, the scatter in the (core excised) $L_X - T_X$ is larger than in the $Y - M$ relation due to the higher sensitivity of the former scaling to the gas physics in the inner regions of clusters.

4.2. Evolution of the scaling relations

In Figs. 2, 3, 4, 5 and 6 we present our findings for the variation with redshift of α (top panels) and $y_0(z)$ (middle panels) for the $T_X - M$, $Y - M$, $Y - T_{\text{mw}}$, $L_X - T_X$ and $Y - L_X$

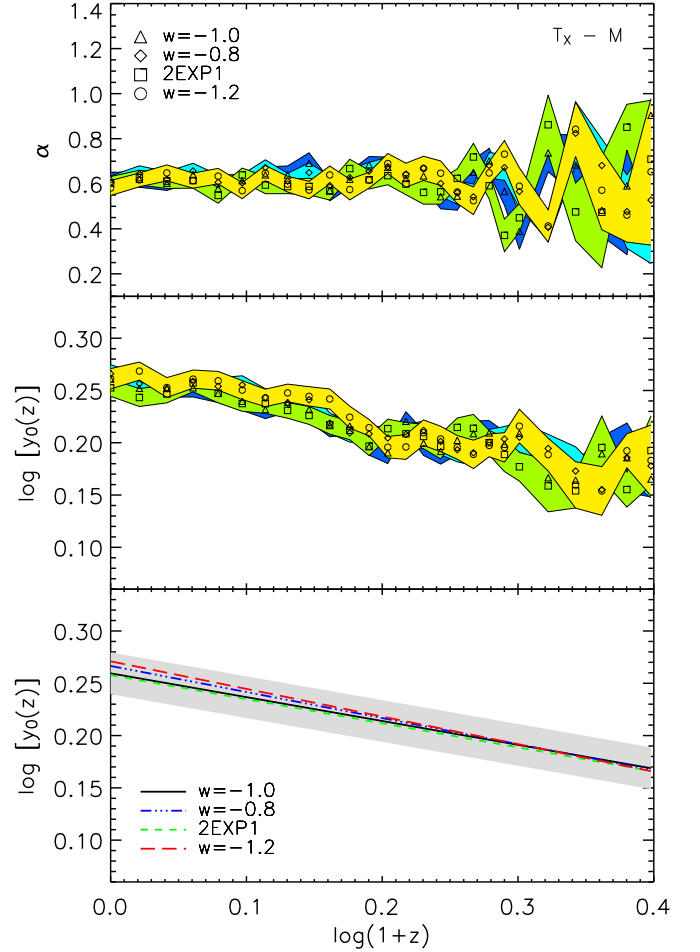


Fig. 2. Slope (upper panel), normalisation $\log(y_0(z))$ (middle panel), and normalisation best fit lines (bottom panel) of the $T_X - M$ relation as a function of redshift ($\log(y_0(z))$ is defined in Eq. 11). Blue colour and triangles stand for the cosmological constant model, cyan and diamonds are for the $w = -0.8$ model, green and squares are for the 2EXP1 model, and yellow and circles are for the $w = -1.2$ model. The shaded area in the bottom panel gives the dispersion of the normalisation fit for the cosmological constant model.

relations, respectively. Here, triangles, diamonds, squares and circles represent the $w = -1$, $w = -0.8$, 2EXP1, and $w = -1.2$ models, respectively. The coloured bands give the the best fit errors obtained at each redshift for these quantities. The lines in the bottom panels of these figures are linear best fits to the evolution of $\log(y_0(z))$ with $\log(1+z)$. The shaded area in these panels gives the rms dispersion of the $\log(y_0(z))$ fit for the cosmological constant model (similar values of dispersion are found for the other models). The resulting best fit parameters for, A , β and α are presented in Table 1, for all scaling investigated in this paper.

As can be inferred from the figures, the fit to a power law, in a redshift range $0 < z < 1.5$, was possible for all the scaling relations explored in the present study except the relations involving L_X (namely $L_X - T_X$ and $Y - L_X$). For the latter two, we found no significant departures of the slopes α from the cosmological constant model but we could not fit the evolution of the scaling relations by a power law within the whole redshift range $0 < z < 1.5$ (see Figs. 5 - 6).

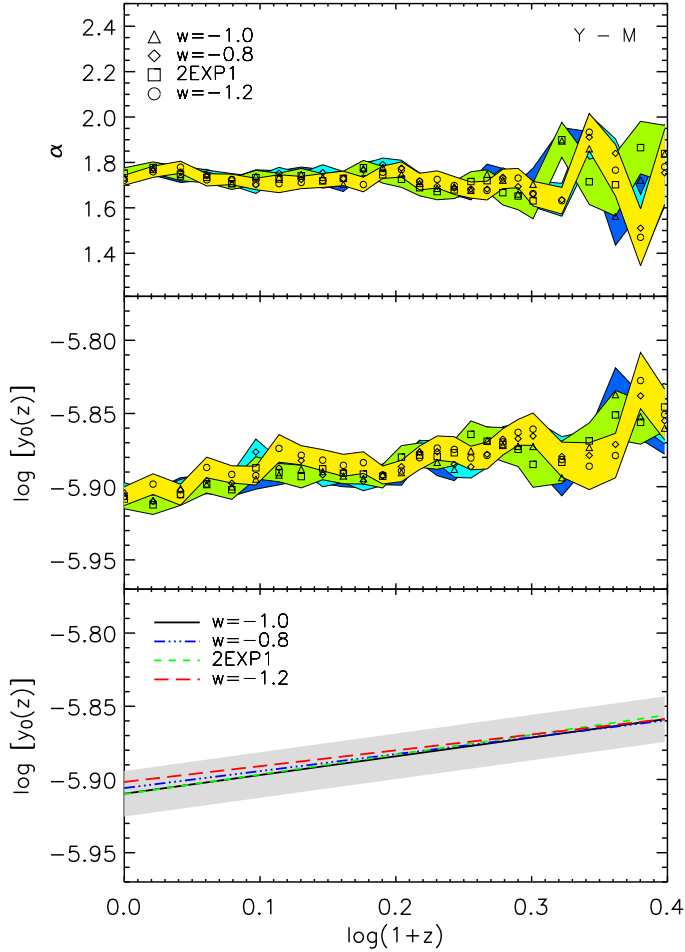


Fig. 3. Slope, normalisation, and normalisation best fit lines of the $Y - M$ relation as a function of redshift. The shaded area in the bottom panel stands for the dispersion of the normalisation for the Lambda model.

For these scalings we therefore restrict the analysis to the a smaller range, namely $0 < z < 0.75$, ie ($\log(1+z) < 0.25$) where the linear fit is valid.

We compared the average value of the slope α of each scaling relation, for all the cosmological models, over the redshift range $0 < z < 1.5$ and found no significant departures from one model to the other, confirming the behavior observed at $z = 0$. This is also clear from the upper panels of Figs. 2, 3, 4, 5 and 6, where there's a high degree of overlap between the α 's obtained for the four cosmological models. For scalings with mass ($T_x - M$ and $Y - M$) the degree of overlap at high redshift is somewhat less striking due to larger variations caused by the rapid decrease of the number clusters with $M_{\text{lim}} > 5 \times 10^{13}$. These “oscillations” show however no systematic dependences with redshift and are about the same “mean values” for all models.

In order to study the evolution of the scaling relations, we factored out the redshift dependence expected from the self-similar evolution which is parametrised by a power law with exponent β , see Eq. (11). As a general remark, we find that, excluding the $T_x - M$ relation, all scalings investigated here show positive evolutions relative to the expected self-similar evolution (i.e. for a given x in Eq (10) the property $y f$ is higher at higher redshift). In the case of

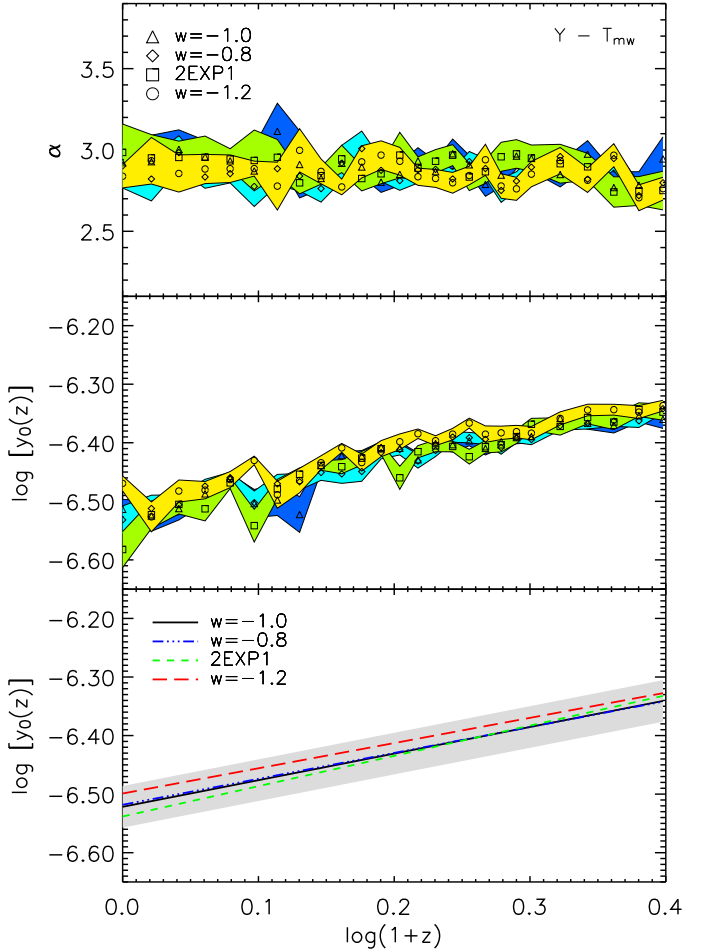


Fig. 4. Slope, normalisation, and normalisation best fit lines of the $Y - T_{\text{mw}}$ relation as a function of redshift. The shaded area in the bottom panel stands for the dispersion of the normalisation for the Lambda model.

$T_x - M$ relation the opposite behaviour is observed. This is expected because the inclusion in all models of radiative cooling (which is a non-gravitational physical process) causes cluster scaling laws to deviate from self-similar evolution, see eg (da Silva et al. 2004; Muanwong et al. 2006) for studies in cosmological constant model simulations.

It is clear from the table and the lower panels of the figures that the value of β is slightly more model dependent than the parameters α and A . This is especially the case for the $L_X - T_x$, and $Y - L_X$ relations for which there is a mild difference between models. For these scalings the $w=-1.2$ and $w=-0.8$ model generally show the largest deviations from the cosmological constant model, whereas the 2EXP1 show the smallest. However, those differences are of the same order as the intrinsic errors and dispersions. We can thus safely consider that there are no significant departures from the cosmological constant model.

5. Conclusions

The abundance of clusters, their redshift distribution, as well as their clustering, are governed by the geometry of the universe and the power spectrum of the initial density perturbations. Gas physics related to cluster structure and

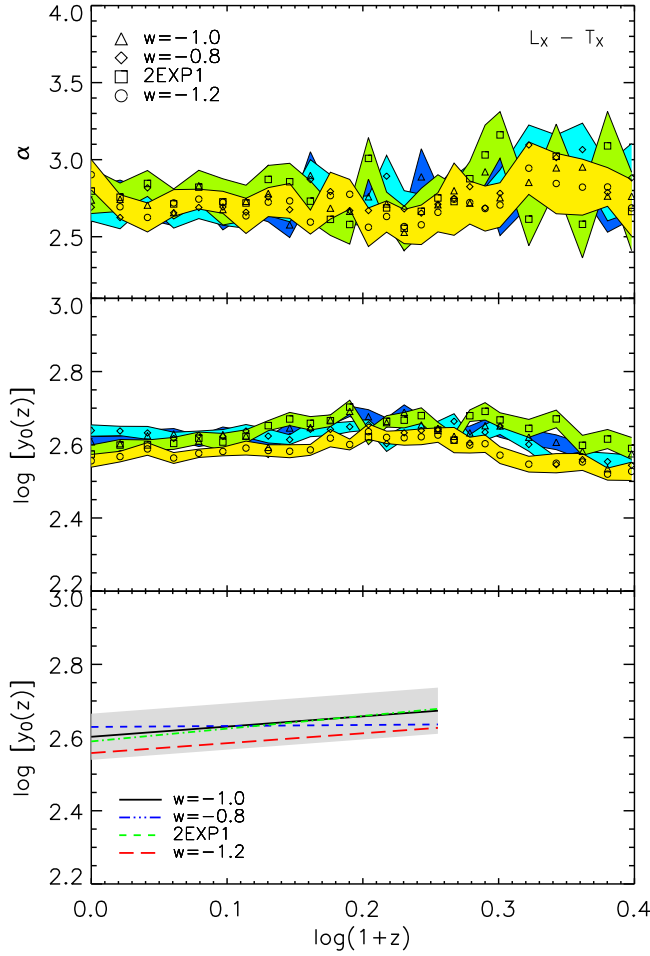


Fig. 5. Slope, normalisation, and normalisation best fit lines of the $L_X - T_X$ relation as a function of redshift. The shaded area in the bottom panel stands for the dispersion of the normalisation for the Lambda model.

evolution also enters through mapping of the cluster observable (SZ flux or X-ray luminosity) relative to the total mass of the cluster. As a result, galaxy cluster counts can be used as probes of cosmological and cluster properties. However, there are several requirements needed to achieve precise cosmological constraints: (i) advances in understanding the formation and evolution of cluster size halos; (ii) a good understanding of the selection function; (iii) robust observational proxies for the cluster mass.

The first condition relates to the conduction of large simulations. This is greatly achieved in the standard cosmological model with a cosmological constant. In the context of dark energy dominated universe, N-body simulations are becoming available for models different from the simple cosmological constant with constant or varying equation of state parameter. These simulations now provide us with a good understanding of the halo properties. They show that the halo mass function is well approximated by the Jenkins mass function. Simulations also indicate that the clusters halos are more concentrated in dark energy models, since structure grow earlier, than in lambda models and that concentrations are higher in models with varying than constant equation state. The second condition, understanding the cluster selection function, translates in understanding

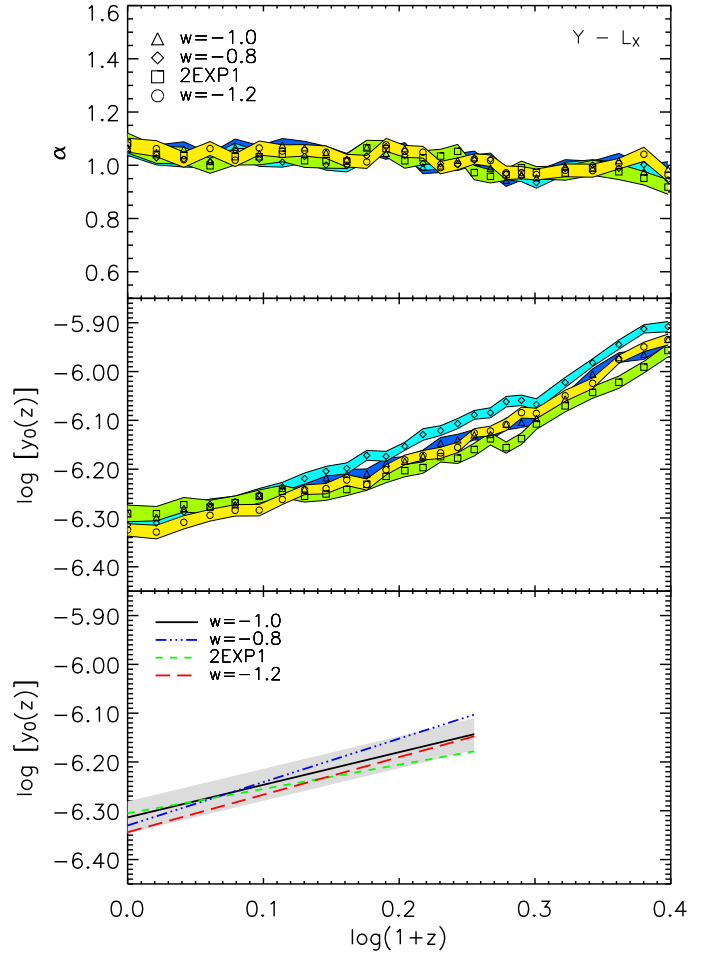


Fig. 6. Slope, normalisation, and normalisation best fit lines of the $Y - L_X$ relation as a function of redshift. The shaded area in the bottom panel stands for the dispersion of the normalisation for the Lambda model.

the limiting mass and the completeness of the surveys from realistic mock cluster catalogues. The mass (or temperature) selection function is directly linked with the cluster observed quantities through cluster scaling relations which is our third requirement (the need for a good proxy for the cluster mass).

In this work we have thus for the first time explored the scaling laws for both SZ and X-rays observations using hydrodynamic simulations of galaxy clusters in four dark energy models with constant or varying equation of states spanning a large class of models. We have studied the scaling properties at $z = 0$ and their evolution with redshift. We have found that dark energy induces no modifications on the scaling laws at $z = 0$ and presents very little differences from the cosmological constant model at higher redshifts.

While detailed simulations incorporating viable dark energy models remains a program in progress, it is reassuring that all models considered in this work predict similar scaling properties to the lambda model. The modeling of the cluster gas component appears to be nearly independent of the dark energy model. Therefore, using the “standard” lambda model scaling relations for converting observable to masses and temperature in future surveys should not in-

introduce any additional bias in the cosmological constraints derived from cluster counts. In this work, we have considered that dark energy does not cluster with dark matter. It would be interesting, however, to evaluate how our conclusions stand for numerical simulations in a scenario where dark energy is inhomogeneous and collapses along with dark matter during the formation of structure. This will be pursued in a forthcoming study.

Acknowledgements. The authors are indebted to Peter Thomas, Orrarujee Muanwong and collaborators for their part in writing the original Sussex cluster extraction software used in this work. We thank Orrarujee Muanwong for discussions and comments on the manuscript. We also acknowledge PAI-PESSOA collaboration program as well as a partial support from the CNES and Programme National de Cosmologie. The simulations used in this study were performed at the IAS computing facilities. NA thanks CAUP for hospitality. AdS acknowledges support from Fundação Ciência e Tecnologia (FCT) under the contracts SFRH/BPD/20583/2004 and CIÊNCIA 2007.

References

- Allen, S.W. & Fabian, A.C. 1998, MNRAS, 297, L57
- Arbey, A., Lesgourgues, J. Salati, P. 2001, Phys. Rev. D, 64, 123528.
- Arnaud, M., Pointecouteau, E., Pratt, G.W., 2005, Astron. & Astrophys., 441, 893.
- Ascasibar, Y., Sevilla, R., Yepes, G., Mueller, V., Gottloeber, S. 2006, M.N.R.A.S., 371, 193.
- Babul, A., Balogh, M.L., Lewis, G.F., Poole, G.B. 2002, MNRAS, 330, 329.
- Bagla, J. S., Jassal, H. K., Padmanabhan, . 2003, Phys. Rev., D67, 063504.
- Balogh, M.L., Babul, A., Voit, M., McCarthy, I.G., Jones, L.R., Lewis, G.F., Ebeling, H. 2006, M.N.R.A.S., 366, 624.
- Bardeen, J. M., Bond, J. R., Kaiser, N., & Szalay, A. S., 1986, ApJ, 304, 15
- Barreiro, T., E. J. Copeland, and N. J. Nunes, 2000, Phys. Rev. D, 61, 127301.
- Bartelmann, M., Doran, M., Wetterich, C. 2005, astro-ph/0507257
- Battye, R. A., and J. Weller, 2003, Phys. Rev., D68, 083506.
- Bean, R., & Magueijo, J. 2002, Phys. Rev., D66, 063505.
- Benson, B.A., Ade, P.A.R., Bock, J.J.
- Bialek, J.J., Evrard, A.E., Mohr, J.J. 2001, ApJ, 555, 597.
- Bonaldi, A., Tormen, G., Dolag, K., Moscardini, L. 2007, astro-ph/0704.2535.
- Borgani, S., et al. 2004, MNRAS, 348, 1078.
- Bryan, G.L. & Norman, M.L. 1998, ApJ, 495, 80.
- Cooray, A.R. 1999, MNRAS, 307, 841.
- Couchman, H. M. P., 1991, ApJ, 368, L23
- Couchman H. M. P., Thomas P. A., Pearce F. R., 1995, MNRAS, 452, 797
- Dolag, K., Bartelmann, M., Perrotta, F., Baccigalupi, C., Moscardini, L., Meneghetti, M., Tormen, G., 2004, MNRAS, 416, 853
- Edge, A.C. & Stewart, G.C. 1991, MNRAS, 252, 414.
- Eke, V. R., Navarro, J. F., & Frenk, C. S., 1998, ApJ, **503**, 569
- Ettori, S., Tozzi, P., Borgani, S., Rosatti, P. 2004, Astron. & Astrophys., 417, 13
- Evrard, A.E., Metzler, C.A. & Navarro, J.F. 1996, ApJ, 469, 494.
- Finoguenov, A., Reiprich, T.H., Bohringer, H. 2001, Astron. & Astrophys., 368, 749.
- Haiman, Z., J. J. Mohr, and G. P. Holder, 2001, Astrophys. J 553, 545.
- Henry, J.P. 2004, ApJ, 609, 603.
- Jenkins, A., Frenk, C. S., White, S. D. M., Colberg, J. M., Cole, S., Evrard, A. E., Couchman, H. M. P., Yoshida, N., 2001, MNRAS, 321, 372
- Kaiser N., 1986, MNRAS, 222, 323
- Kay, S.T., da Silva, A.C., Aghanim, N., Blanchard, A., Liddle, A.R.
- Puget, J.-L., Sadat, R., Thomas, P.A. 2007, MNRAS,
- Klypin, A., Maccio, A. V., Mainini, R., Bonometto, S. A. 2003, ApJ, 599, 31.
- Kuhlen, M., Strigari, L. E., Zentner, A. R., Bullock, J. S., Primack, J. R. 2004, astro-ph/0402210.
- Linder, E. V. & Jenkins, J. 2003, astro-ph/0305286.
- Lokas, E. L., Bode, P., Hoffman, Y. 2003, astro-ph/0309485.
- Maio, U., Dolag, K., Meneghetti, M., Moscardini, L., Yoshida, N., Baccigalupi, C., Bartelmann, M., Perrotta, F., 2006, MNRAS, 373, 869
- Manera, M., Mota, D. F. 2006 MNRAS, 371, 1373.
- Markevitch, M. 1998, ApJ, 504, 27.
- Maughan, B.J., Jones, L.R., Ebeling, H., Scharf, C. 2006, MNRAS, 365, 509.
- McCarthy, I.G., Babul, A., Holder, G.P., Balogh, M.L. 2003, ApJ, 591, 515.
- Meneghetti, M., Jain, B., Bartelmann, M., Dolag, K., 2005, MNRAS, 362, 1301
- Meneghetti, M., Bartelmann, M., Dolag, K., Perrotta, F., Baccigalupi, C., Moscardini, L., Tormen, G., 2005, Astron. & Astrophys., 442, 413
- Mohr, J. J., 2004, astro-ph/0408484.
- Molt, P.M., Hallman, E.J., Burns, J.O., Norman, M.L. 2005, ApJ, 623, L63.
- Monaghan, J. J., 1992, Ann. Rev. Astron. Astrophys., 30, 543
- Morandi, A., Ettori, S., Moscardini, L. 2007 astro-ph/0704.2678.
- Muanwong, O., Thomas, P.A. Kay, S.T., Pearce, F.R., Couchman, H.M.P. 2001, ApJ, 552, L27.
- Muanwong O., Thomas P. A., Kay S. T., Pearce F. R., 2002, MNRAS, 336, 527
- Muanwong, O., Kay, S.T., Thomas, P.A. 2006, ApJ, 649, 640.
- Nevalainen, J., Markevitch, M., Forman, W. 2000, ApJ, 532, 694.
- Nunes, N. J., and D. F. Mota, 2006, M.N.R.A.S., 368, 751.
- Nunes, N. J., da Silva, A.C., Aghanim, N. 2006, Astron. & Astrophys., 450, 899.
- Padmanabhan, T. & Choudhury, T.R. 2002, Phys. Rev., D66, 081301.
- Pearce F. R., Couchman H. M. P., 1997, New Astronomy, 2, 411
- Pearce F. R., Thomas P. A., Couchman H. M. P., Edge A. C., 2000, MNRAS, 317, 1029
- Perlmutter, S. et al. 1999, ApJ, 517, 565.
- Rasia, E., Mazzotta, P., Borgani, S., Moscardini, L., Dolag, K., Tormen, G., Diaferio, A., Murante, G. 2005, ApJ, 618, L1.
- Riess, A. G. et al. 1998, AJ, 116, 1009.
- Rowley, D.R., Thomas, P.A. & Kay, S.T. 2004, MNRAS, 352, 508.
- da Silva A. C., Barbosa D., Liddle A. R., Thomas P. A., 2000, MNRAS, 317, 37
- da Silva A. C., Barbosa D., Liddle A. R., Thomas P. A., 2001, MNRAS, 326, 155
- da Silva, A.C., Kay, S.T., Liddle, A.R., Thomas, P.A. 2004, M.N.R.A.S., 348, 1401
- Sugiyama, N., 1995, Astrophys.J.Suppl., 100, 281
- Sunyaev R. A., Zel'dovich Ya. B., 1972, Comm. Astrophys. Space Phys., 4, 173
- Sunyaev R. A., Zel'dovich Ya. B., 1980, ARA&A, 18, 537
- Sutherland R. S., Dopita M. A., 1993, ApJS, 88, 253
- Thacker R. J., Couchman H. M. P., 2000, ApJ, 545, 728
- Thomas P. A., Couchman H. M. P., 1992, MNRAS, 257, 11
- Thomas P. A. et al. (the Virgo Consortium), 1998, MNRAS, 296, 1061
- Thomas, P.A., Muanwong, O., Pearce, F.R., Couchman, H.M.P., Edge, A.C., Jenkins, A., Onuora, L. 2001, MNRAS, 324, 450
- Voit, G.M., Bryan, G.L., Balogh, M.L., Bower, R.G. 2002, ApJ, 576, 601.
- Wang, S., J. Khoury, Z. Haiman, and M. May, 2004, Phys. Rev. D 70, 123008.
- Weinberg, N. N., & M. Kamionkowski, 2003, M.N.R.A.S., 341, 251.
- Weller, J., R. Battye, and R. Kneissl, 2002, Phys. Rev. Lett., 88, 231301.

Table 1. Best fit values of the parameters α , $\log A$ and β as well as their respective 1σ errors. These values are valid within the redshift range $0 < z < 1.5$. For the $L_X - T_X$ and $Y - L_X$ relations, the linear fit and the associated parameters are only valid in the range $0 < z < 0.75$ above which the linear fit is not a good approximation.

Model		$w = -1$	$w = -0.8$	2EXP1	$w = -1.2$
$T_X - M$	α_{TM}	0.620 ± 0.029	0.604 ± 0.031	0.581 ± 0.033	0.602 ± 0.029
	$\log A_{\text{TM}}$	0.260 ± 0.005	0.267 ± 0.004	0.271 ± 0.005	0.258 ± 0.005
	β_{TM}	-0.228 ± 0.020	-0.249 ± 0.017	-0.264 ± 0.023	-0.230 ± 0.023
$Y - M$	α_{YM}	1.732 ± 0.025	1.730 ± 0.025	1.721 ± 0.022	1.752 ± 0.024
	$\log A_{\text{YM}}$	-5.910 ± 0.004	-5.906 ± 0.004	-5.902 ± 0.005	-5.910 ± 0.003
	β_{YM}	0.128 ± 0.016	0.116 ± 0.016	0.108 ± 0.020	0.135 ± 0.013
$Y - T_{\text{mw}}$	α_{YT}	2.922 ± 0.100	2.902 ± 0.136	2.838 ± 0.072	2.985 ± 0.175
	$\log A_{\text{YT}}$	-6.522 ± 0.008	-6.518 ± 0.005	-6.499 ± 0.007	-6.538 ± 0.008
	β_{YT}	0.454 ± 0.036	0.443 ± 0.022	0.430 ± 0.031	0.517 ± 0.036
$L_X - T_X$	α_{LT}	2.738 ± 0.086	2.691 ± 0.089	2.902 ± 0.099	2.796 ± 0.146
	$\log A_{\text{LT}}$	2.602 ± 0.010	2.629 ± 0.007	2.558 ± 0.006	2.589 ± 0.011
	β_{LT}	0.279 ± 0.063	0.027 ± 0.042	0.270 ± 0.035	0.348 ± 0.070
$Y - L_X$	α_{YL}	1.063 ± 0.028	1.064 ± 0.026	1.076 ± 0.026	1.084 ± 0.037
	$\log A_{\text{YL}}$	-6.314 ± 0.005	-6.330 ± 0.004	-6.344 ± 0.005	-6.305 ± 0.006
	β_{YL}	0.668 ± 0.033	0.890 ± 0.028	0.770 ± 0.034	0.497 ± 0.037